Corrosion Science 82 (2014) 67–76

Contents lists available at ScienceDirect

Corrosion Science

journal homepage: www.elsevier.com/locate/corsci

Corrosion behavior of an alumina forming austenitic steel exposed to supercritical carbon dioxide

Ling-Feng He *, Paul Roman, Bin Leng, Kumar Sridharan *, Mark Anderson, Todd R. Allen

Department of Engineering Physics, University of Wisconsin-Madison, WI 53706, USA

ARTICLE INFO

Article history:
Received 31 October 2013
Accepted 31 December 2013
Available online 8 January 2014

Keywords:
A. Stainless steels
B. SEM
B. STEM
C. High temperature corrosion
C. Oxidation
C. Carburization

ABSTRACT

Microstructure characterization of corrosion behavior of an alumina forming austenitic (AFA) steel exposed to supercritical carbon dioxide was conducted at 450–650 °C and 20 MPa. At low temperature and short exposure times, the oxidation kinetics were parabolic and the oxide scales were mainly composed of protective and continuous Al_2O_3 and (Cr, Mn)-rich oxide layers. As the temperature and exposure time increased, the AFA steel gradually suffered breakaway oxidation and its oxide scales showed a multilayer structure mainly composed of Fe_3O_4, $(Cr, Fe)_3O_4$, $NiFe/FeCr_2O_4/Cr_2O_3/Al_2O_3$, $FeCr_2O_4/Al_2O_3$, and $NiFe/Cr_2O_3/Al_2O_3$, in sequence. The corrosion mechanism based on the microstructure evolution is discussed in detail.

Published by Elsevier Ltd.

1. Introduction

The goal of this study was to investigate materials corrosion issues in high temperature sections of the supercritical carbon dioxide (SC-CO_2) Brayton cycle for power conversion system in a Generation IV Fast Reactor [1,2]. The temperatures of SC-CO_2 in the recuperator, reactor, turbine, and generator sections can be quite high (about 400–650 °C). Additionally, the SC-CO_2 operated in a closed-loop recompression Brayton cycle also offers the potential of equivalent or higher cycle efficiency versus supercritical or superheated steam cycles at temperatures relevant for concentrating solar power (CSP) applications [3]. CSP plants are required to operate at 600–900 °C to improve the power conversion efficiencies. Materials corrosion primarily at these high temperatures will be an important issue, particularly because the expected life times of these components will be 20 years or higher. Additionally, the formation of thick corrosion product oxide layers can impede heat transfer capability in components such as the heat exchanger. Therefore, a detailed knowledge of the corrosion mechanism and rates of microstructure degradation is important to estimate the lifetime of the component and define mitigation strategies for improved corrosion performance of alloys.

The alumina forming austenitic (AFA) steels were developed at Oak Ridge National Laboratory, which exhibit a unique combination of high-temperature creep strength through the formation of stable nano NbC and submicron B_2-NiAl and Fe_2Nb base Laves precipitate and oxidation resistance via protective alumina scale formation [4–9]. Since Al_2O_3 scales have lower growth rates and show better thermodynamically stability when compared to Cr_2O_3 scales [6], which form on conventional stainless steels, AFA steels hold the potential to permit significantly increased operating temperatures in high-temperature oxidizing environments. Also, the Al_2O_3 scales have proven to be particularly protective in the presence of aggressive carbon- or sulfur-species and water vapor [10–12]. It follows that AFA steels show good corrosion resistance in various simulated environments (sulfidation-oxidation, metal dusting, steam and air with 10% water vapor) for chemical processing and energy production applications [13,14]. It has also been shown that the oxidation resistance of the AFA steels in supercritical water was superior to other austenitic alloys, 800H, D9, and 316 stainless steels tested under similar conditions due to the formation of a protective Al–Cr–Fe-rich oxide layer [15].

In this work, the corrosion behavior of an AFA steel was studied in SC-CO_2 at 450–650 °C and 20 MPa, and its multi-scale microstructure and composition were investigated by scanning electron microscope (SEM) and advanced analytical transmission electron microscopy (TEM).

2. Experimental procedure

2.1. Corrosion tests

The composition (in wt.%) of AFA-OC 6 steel (referred to as AFA hereon) is listed in Table 1. Raw material was provided in plate

* Corresponding authors. Tel.: +1 608 263 4789; fax: +1 608 263 7451.
E-mail addresses: lhe33@wisc.edu (L.-F. He), kumar@engr.wisc.edu (K. Sridharan).

0010-938X/$ - see front matter Published by Elsevier Ltd.
http://dx.doi.org/10.1016/j.corsci.2013.12.023

form and was solution heat-treated. The material was cut using the electrical discharge machining (EDM) technique to yield square test coupon geometry of 12.7 mm × 12.7 mm × 1.5 mm. A 3 mm hole was drilled through the upper corner of each specimen for test mounting purposes. Prior to corrosion testing, all surfaces of the coupons were carefully ground with 800 grit SiC paper. To minimize the possibility of preferential attack at the edges, the edges were rounded off slightly using 600 grit SiC paper. After obtaining the desired surface finish each coupon was measured using a micrometer (±0.001 mm) and weighed (±2 μg) to determine weight change per unit area after oxidation. Finally, all coupons were cleaned in an ethanol solution using an ultrasonic agitator.

For corrosion tests, the autoclave temperature was raised from atmospheric conditions to the desired temperature (450 °C, 550 °C, or 650 °C). Research grade CO_2 (99.998%) was fed in a liquid state from a commercial cylinder (70 °F, ~835 psi) to a SC-CO_2 pump, which pumped the liquid to a gas beyond its critical pressure (7.39 MPa) to 20 MPa. A pre-heat line, just after the pump outlet, heated the gas to minimize any thermal disparity as it enters the autoclave above its critical temperature (31 °C). Tubes were welded into holes in the body of the autoclave to allow access for three thermocouples and a pressure sensor to monitor environmental conditions using LabVIEW hardware and software. At these particular supercritical conditions, the thermodynamic properties of SC-CO_2 for proposed Brayon Cycle design layouts provides very high cycle efficiency due to less compression, which also promotes smaller turbomachinery. The coupons, which are suspended on an alumina sample holder, were positioned approximately in the center of the autoclave. The flow rate of SC-CO_2 was about 0.02 kg/hr, sufficient to refresh the autoclave every two hours, and can be considered as low flow or quasi-static. The SC-CO_2 is then returned to atmospheric conditions after 200 h of exposure to enable removal of coupons for weighing and determination of weight change. A total of ten coupons were tested, with two coupons being removed every 200 h of exposure for surface analysis. Gas composition from the cylinder and the autoclave outlet was monitored using a mass spectrometer (MS) system. A schematic process flow diagram of the SC-CO_2 test setup is shown below in Fig 1. This system has also been employed to study the corrosion behavior of stainless steels and nickel-based alloys [16–19].

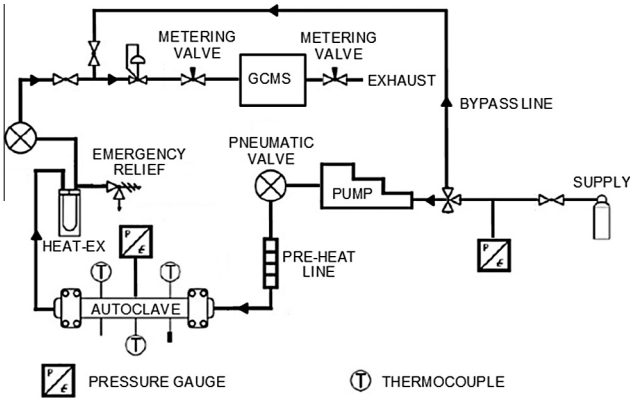

Fig. 1. Schematic of the SC-CO_2 corrosion test setup used in the present study.

2.2. Microstructural characterization

The cross section samples for SEM observation were cut from as-oxidized samples. Prior to cutting the specimens, a copper plating was deposited electrochemically onto the surface to minimize the distortion of surface features during mechanical polishing and to improve the contrast during SEM observation. The Cu-plated specimens were encapsulated in a thermosetting resin, mechanically ground down with 1200 grit SiC paper and polished using 0.01 μm silica suspension.

TEM samples were prepared in a Zeiss 1500XB focused ion beam (FIB) system. Platinum coating was deposited to protect the oxide surface before cutting. TEM lamellae were created by coarse trenching to produce samples 20 μm × 15 μm × 1 μm in dimensions using the FIB technique. The samples were then welded to a copper TEM grid for final thinning. The samples were thinned to a final thickness of roughly 100 nm using 30 kV gallium ions and further polished using 5 kV gallium ions. The TEM lamellae were finally cleaned with a Fischione's Model 1040 Nanomill with 900 eV Ar ions for 30 min for each side.

A LEO 1500 field emission SEM equipped with an energy-dispersive spectrometer (EDS) system was used to study the morphology and compositions of both surface and cross section of corroded samples. A Titan scanning transmission electron microscope (STEM) with CEOS probe aberration corrector operated at 200 kV, equipped with a high-angle angular-dark-field (HAADF) detector and EDS system, was used for electron diffraction, high-resolution scanning transmission electron microscopy (HRSTEM) imaging and composition analysis. The probe size for EDS line-scan is less than 1 nm and step size about 1 nm. Electron energy loss spectroscopy (EELS) was employed to study the composition and microchemistry of oxide scales. The EELS spectrum images were taken in energy filtered STEM mode with 24.5 mrad convergence angle, 52 mrad collection angle and 0.8 eV energy resolution.

3. Results

3.1. Weight gain and morphology

At 450 °C, weight changes due to oxidation were low in magnitude, but obeyed the parabolic growth rate law, typically characteristic of the presence of an inner compact and protective oxide layer (Fig. 2). However, the kinetics of oxidation transformed from a parabolic to a linear growth rate law as the test temperature increased. The oxidation curve at 550 °C indicates a trend that is initially linear through an inflection point at 600 h and grows exponentially thereafter. This particular transition in rates is a result of breakaway oxidation. Similar transitions in oxidation behavior have been described earlier in other oxidizing environments [20–24]. It has commonly been suggested that transition to breakaway oxidation is a result of cracking of the oxide layer. At 650 °C, the oxidation behavior could be described by a combination of rate equations resembling that of an S-shaped curve. The reaction changes abruptly, exhibiting a ballooning effect between 400 and 600 h of exposure, after which some healing of the oxide layer takes effect, but it is still nonprotective at longer exposure times. The surface morphology and cross section microstructure

Table 1
Element compositions (wt.%) in AFA-OC 6.

Fe	Ni	Cr	Al	Nb	Mn	Cu	Mo	W	Si	C	Ti	V	P	B	N
51.83	25.04	13.84	3.56	2.51	1.99	0.51	0.18	0.16	0.13	0.114	0.05	0.05	0.022	0.008	0.001